



RESEARCH PAPER

# Characterizing 3D inflorescence architecture in grapevine using X-ray imaging and advanced morphometrics: implications for understanding cluster density

Mao Li<sup>1, ID</sup>, Laura L. Klein<sup>1,2</sup>, Keith E. Duncan<sup>1, ID</sup>, Ni Jiang<sup>1</sup>, Daniel H. Chitwood<sup>3,4, ID</sup>, Jason P. Londo<sup>5</sup>, Allison J. Miller<sup>1,2, ID</sup> and Christopher N. Topp<sup>1,\* ID</sup>

<sup>1</sup> Donald Danforth Plant Science Center, 975 North Warson Road, St Louis, MO 63132-2918, USA

<sup>2</sup> Department of Biology, Saint Louis University, 3507 Laclede Avenue, St Louis, MO 63103-2010, USA

<sup>3</sup> Department of Horticulture, Michigan State University, East Lansing, MI 48824, USA

<sup>4</sup> Department of Computational Mathematics, Science and Engineering, Michigan State University, East Lansing, MI 48824, USA

<sup>5</sup> United States Department of Agriculture, Agricultural Research Service: Grape Genetics Research Unit, 630 West North Street, Geneva, NY 14456-1371, USA

\* Correspondence: [ctopp@danforthcenter.org](mailto:ctopp@danforthcenter.org)

Received 28 February 2019; Editorial decision 13 August 2019; Accepted 21 August 2019

Editor: Roland Pieruschka, Forschungszentrum Jülich, Germany

## Abstract

Inflorescence architecture provides the scaffold on which flowers and fruits develop, and consequently is a primary trait under investigation in many crop systems. Yet the challenge remains to analyse these complex 3D branching structures with appropriate tools. High information content datasets are required to represent the actual structure and facilitate full analysis of both the geometric and the topological features relevant to phenotypic variation in order to clarify evolutionary and developmental inflorescence patterns. We combined advanced imaging (X-ray tomography) and computational approaches (topological and geometric data analysis and structural simulations) to comprehensively characterize grapevine inflorescence architecture (the rachis and all branches without berries) among 10 wild *Vitis* species. Clustering and correlation analyses revealed unexpected relationships, for example pedicel branch angles were largely independent of other traits. We identified multivariate traits that typified species, which allowed us to classify species with 78.3% accuracy, versus 10% by chance. Twelve traits had strong signals across phylogenetic clades, providing insight into the evolution of inflorescence architecture. We provide an advanced framework to quantify 3D inflorescence and other branched plant structures that can be used to tease apart subtle, heritable features for a better understanding of genetic and environmental effects on plant phenotypes.

**Keywords:** 3D architecture, inflorescence, morphology, persistent homology, phylogenetic analysis, topological data analysis, *Vitis* spp., X-ray tomography.

## Introduction

Inflorescences are a major feature of the angiosperm lineage whose architectural variation affects fertilization, fruit development, dispersal, and crop yield (Wyatt, 1982; Hake, 2008; de Ribou *et al.*, 2013; Kirchoff & Claßen-Bockhoff, 2013; Périlleux *et al.*, 2014; Chanderbali *et al.*, 2016). These branched reproductive structures with multiple flowers reflect

© The Author(s) 2019. Published by Oxford University Press on behalf of the Society for Experimental Biology.

This is an Open Access article distributed under the terms of the Creative Commons Attribution Non-Commercial License (<http://creativecommons.org/licenses/by-nc/4.0/>), which permits non-commercial re-use, distribution, and reproduction in any medium, provided the original work is properly cited. For commercial re-use, please contact journals.permissions@oup.com

the extraordinary diversity across angiosperm species, from an ear of corn to palms with inflorescences measuring 5 m long (Hodel *et al.*, 2015). Yet seemingly simple processes give rise to these vastly different shapes—during development reproductive meristems may either switch to floral identity or proliferate additional inflorescence meristems and branches (Prusinkiewicz *et al.*, 2007). However, such complex topologies have proven difficult to quantify with conventional tools.

Detailed descriptions of inflorescences by trained experts are often unique to specific research communities or groups of taxa, and are not always readily transferable, hindering meaningful comparative analysis (Endress, 2010). Inflorescences are sometimes described typologically: indeterminate or determinate, simple or compound, as a raceme, cyme, panicle or spike, etc. (Wyatt, 1982; Weberling, 1992). Other approaches describe qualitative attributes of inflorescences such as the presence or absence of certain structures, such as secondary branches or bracts (Weberling, 1992; Doebley *et al.*, 1997; Feng *et al.*, 2011; Hertweck & Pires, 2014). A third method for characterizing inflorescences is through quantification of component structures (e.g. branch length, inflorescence length and width, angular traits; Kuijt, 1981; Marguerit *et al.*, 2009; Landrein *et al.*, 2012; Le *et al.*, 2018). Although these classical quantitative approaches facilitate comparative statistical analyses, the three-dimensional (3D) complexity of inflorescences is largely undescribed. Furthermore, descriptions may be confounded by developmental stage at the time of measurement, and distinguishing between vegetative and reproductive branching structures can be difficult (Wyatt, 1982; Weberling, 1992; Guédon *et al.*, 2001). Thus, new technological and analytical approaches that can represent comprehensive, multi-dimensional information about inflorescence diversity are needed to normalize and enrich analysis of these structures.

One promising approach for capturing 3D shapes of inflorescences and other plant structures is X-ray tomography (XRT). XRT generates high quality reconstructions of the internal and external shapes of plants, preserving nearly complete geometric and topological information in 3D. These 3D digital models then can be used to extract quantitative data (features) from plant structures. X-rays have been used to quantify wheat and rice seed and inflorescence traits from intact samples for non-destructive yield calculations (Jhala & Thaker, 2015; Hughes *et al.*, 2017), internal anatomy of willow trees (Brereton *et al.*, 2015), stem morphology and anatomy in sorghum (Gomez *et al.*, 2018), root structure of barley seedlings (Pfeifer *et al.*, 2015), leaf anatomy in monocots and dicots (Mathers *et al.*, 2018), and dynamic starch accumulation in living grapevine stems (Earles *et al.*, 2018), among others. Most critically, whereas manual measurements can be laborious and destructive, non-destructive sampling for XRT analysis facilitates comprehensive quantification of complex morphological traits.

Quantifying complex shapes with XRT requires appropriate analytical approaches. Topological modeling, a mathematical field concerned with the connectedness of branching structures, can quantify inflorescence architecture by parsing geometric 3D structures into distinct, yet connected, components (Godin & Caraglio, 1998). Topological modeling has yielded important insights into inflorescence

development, functional analysis, and crop improvement in a variety of plant species (e.g. *Arabidopsis thaliana*, *Capsicum annuum*, *Malus pumila*, and *Triticum*; Godin *et al.*, 1999; Letort *et al.*, 2006; Kang *et al.*, 2009). While powerful, these reductionist approaches rely on an *a priori* understanding of the mechanisms that contribute to complexity (e.g. branching patterns), and lose power when shapes vary drastically from one another (e.g. comparing a corn tassel to a grape cluster). Approaches that capture emergent properties of complex structures without presupposing the importance of individual structural components are complementary to traditional topological models (Bucksch *et al.*, 2017).

An emerging mathematical approach to interpret topological models is persistent homology (PH). PH extracts morphological features from two- or three-dimensional representations and can be used to compare very different shapes. PH has been applied to explain a wide range of features including atomic structures, urban and forested areas, cancers, cell shapes, and jaw shape, among others (Edelsbrunner & Morozov, 2013). In plants, PH has been used to estimate shapes that are otherwise difficult to measure including leaves, leaflet serration, spikelet shape, stomatal patterning, and root architecture (Haus *et al.*, 2018; Li *et al.*, 2018a,b; Migicovsky *et al.*, 2017; McAllister *et al.*, 2019). Previous work showed that PH could capture more quantitative variation than traditional plant morphological measures (described above) resulting in the identification of otherwise latent quantitative trait loci (Li *et al.*, 2018b). PH is especially well-suited for quantifying branching topology as it can quantitatively summarize complex variation with a single measure (Li *et al.*, 2017; Delory *et al.*, 2018). Rachis, pedicel, and branches include inherently topological features that can be especially well-analysed with PH-based methods.

Grape clusters (or bunches) are branched structures supporting berries produced by grapevines (*Vitis* spp.) and are an ideal system in which to apply XRT and PH. Grape infructescences are historically, culturally, and economically important and vary extensively in nature and in cultivation (Iland *et al.*, 2011). Cluster architecture determines bunch density, which is described as ‘arrangement of berries in a cluster and the distribution of free space’ (Richter *et al.*, 2019). The density of berries in a cluster is an important breeding feature because it determines yield, wine character, and disease resistance (amount of air flow between berries is a primary determinant of pests and pathogens on the fruit). Cluster density is a characteristic identified by the Organization Internationale de la Vigne et du Vin, and varies from ‘berries clearly separated’ (loose clusters) to ‘berries deformed by compression’ (very dense clusters; OIV, 2001). As primary determinants of yield, end-product characteristics and disease resistance cluster architecture have been studied extensively in grapevine (reviewed in Tello & Ibáñez, 2018). These studies have shown that wine grape cultivars (*Vitis vinifera*) display distinct bunch densities (Shavrukov *et al.*, 2004). However, less is known about cluster architecture in wild *Vitis* species, an important source of natural variation used by breeders in the development of hybrid grapevine varieties.

Historically, researchers have focused on a suite of cluster traits such as cluster size, shape, weight, and density/

compactness to characterize bunch density quantified in grapevines (Rovasenda, 1881; Pulliat, 1888; Bioletti, 1938; Galet, 1979; Bettiga, 2003). Measurements are made primarily using traditional tools including rulers, digital calipers, volume displacement, and/or through human judging panels. More recently, automated image-based approaches have been implemented to capture aspects of cluster architecture in the lab and field (Ivorra *et al.*, 2015; Aquino *et al.*, 2017, 2018; Rist *et al.*, 2018). However, these image-based methods cannot penetrate the internal inflorescence structure. Therefore resulting models are based only on the visible surface and the underlying topology cannot be fully captured, limiting an understanding of how inflorescence architecture and berry features co-vary. XRT and PH applications offer an important opportunity to understand grapevine bunch density through detailed analyses of inflorescence architecture. This work will deepen our understanding of natural variation of inflorescence structure, identify priority targets for breeding, and permit connecting 3D structure to underlying processes and genetics of inflorescence development.

We used X-ray tomography, geometric measurements, persistent homology, and structural simulation to characterize wild grapevine inflorescence architecture. We targeted the branching architecture of the mature inflorescence: the rachis and all branches that remain following the removal of ripe berries (Fig. 1). Specifically, we aimed to: (i) characterize variation in component traits of inflorescence architecture within and among *Vitis* species; (ii) assess phylogenetic signals underlying inflorescence architecture traits; and (iii) interpret inflorescence trait variation in the context of breeding objectives. This work represents an important advance for the characterization of 3D plant architecture using a powerful combined imaging and computational approach.

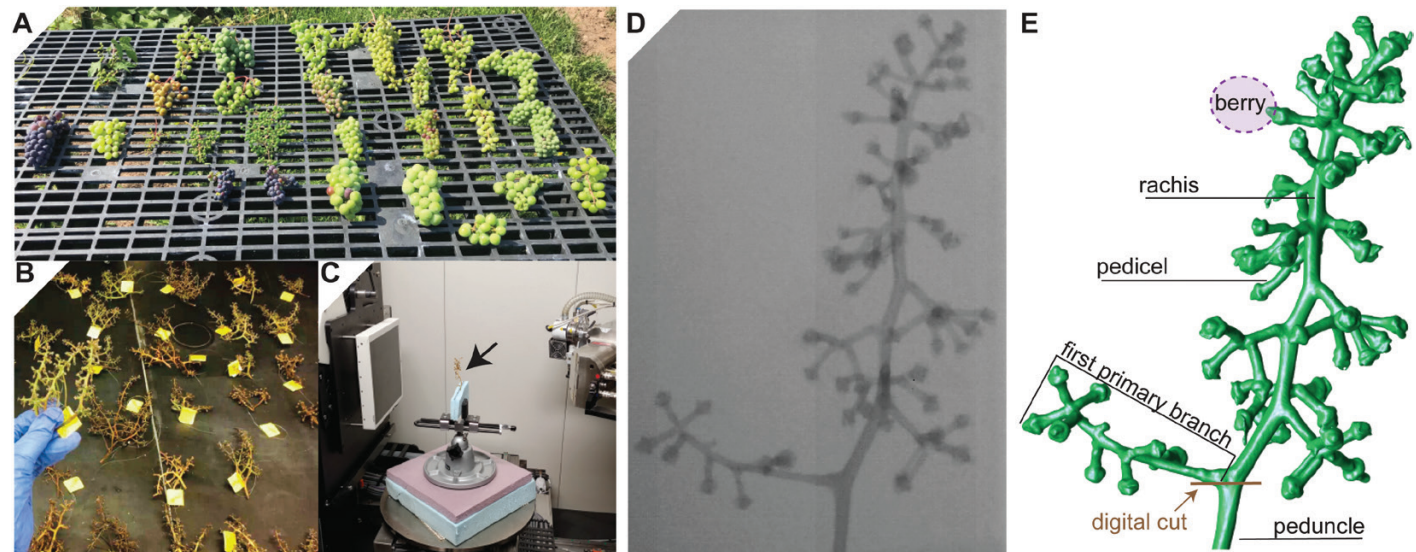


**Fig. 1.** Sample preparation and imaging. (A) The 10 *Vitis* species sampled for this study displayed diverse grape bunch morphology. (B) Inflorescence architectures after berry removal. (C) Inside the X-ray tomography instrument; the inflorescence is clamped in a portable clamping device between two pieces of polystyrene on the X-ray turntable. (D) Two dimensional radiograph of grape inflorescence; X-rays, absorbed or passing through the inflorescence, are detected to create a silhouette. (E) Three dimensional reconstruction and the structure of the same inflorescence shown in (D) by taking radiographs at successive different angles and then computationally combining the images.

## Materials and methods

### Plant material

In this study, we sampled grapevine bunches from 136 unique genotypes representing 10 wild *Vitis* species living in the USDA germplasm repository system (Geneva, NY, USA; Table 1; Supplementary Fig. S1 at JXB online). Grapevines have a paniculate inflorescence that consists of a rachis with several primary and secondary branches, tapering towards the terminus of the organ (Ilard *et al.*, 2011). Wild grapevines are dioecious; consequently, unbalanced sample sizes for different species reflect numbers of female genotypes available in the germplasm collection. Each unique genotype is represented in the germplasm collection by two clonally replicated vines. For most of the 136 genotypes, we collected a total of three clusters from the two clonal replicates combined, representing average cluster morphology. We avoided clusters that were visibly damaged or indirectly altered (e.g. tendril or trellis interference). For each vine, clusters were removed from separate canes at the point of peduncle attachment (Fig. 1A). In total, 392 clusters were collected in September 2016 when berries were soft, equivalent to EL38 developmental stage (Coombe, 1995; Fig. 1A). Berries were manually removed from clusters in the field, and the remaining inflorescence stalks (including rachis, branches, and pedicels; hereafter referred to as inflorescence or inflorescence architecture) were used to assess inflorescence architecture (Fig. 1B).

### X-ray tomography and data preprocessing

Grapevine inflorescences were scanned at the Donald Danforth Plant Science Center (St Louis, MO, USA) using a North Star Imaging X5000 X-ray tomography instrument (NSI; Rogers, MN, USA) equipped with a 16-bit Varian flat panel detector ( $1536 \times 1920$  pixels with  $127 \mu\text{m}$  pixel pitch) and 225 kV microfocus reflection target X-ray source. Each inflorescence was held between two pieces of construction-grade expanded polystyrene, clamped in a portable clamping device, and positioned on the X-ray turntable in one of two configurations (Fig. 1C): 725 mm from the source, generating  $\times 1.26$  magnification and  $101 \mu\text{m}$  voxel resolution, or 766 mm from the source, generating  $\times 1.19$  magnification and  $107 \mu\text{m}$  voxel resolution. Each scan used X-ray power set to 60 kV and 1200  $\mu\text{A}$  at 10 frames per second, collecting 1200 16-bit TIFF projections over  $360^\circ$  of rotation during a 2 min continuous standard scan. Projections for each scan (Fig. 1D) were combined into a single 3D volume using NSI efX-CT software, converted to a density-based surface rendering

**Table 1.** Number of samples/individuals of each species and berry information used in the study

Species	Number			Berry information <sup>a</sup>		
	Samples	Individuals	Individuals used in phylogenetic analysis	Low diameter (mm)	High diameter (mm)	Berries per bunch
<i>V. acerifolia</i>	32	11	9	8	12	>25
<i>V. aestivalis</i>	5	2	1	8	20	>25
<i>V. amurensis</i>	13	5	2	8	15	NA
<i>V. cinerea</i>	45	15	13	4	8	>25
<i>V. coignetiae</i>	6	2	1	NA	8	NA
<i>V. labrusca</i>	62	22	12	12	23	<25
<i>V. palmata</i>	3	1	1	8	10	>25
<i>V. riparia</i>	158	53	48	8	12	>25
<i>V. rupestris</i>	41	16	10	8	12	<25
<i>V. vulpina</i>	27	9	2	8	12	>25
Total	392	136	99			

NA, not available.

<sup>a</sup> Berry information is from Galet (1988) and Moore and Wen (2016).

Polygon file (PLY), and exported for analysis (Fig. 1E). The full PLY dataset for this work is 7.85 GB, and can be downloaded from: <https://www.danforthcenter.org/scientists-research/principal-investigators/chris-topp/resources>.

We exported the surface mesh data (.ply files) into Meshlab (v1.3.3; Cignoni *et al.*, 2008) and performed the following processing steps to remove topological noise: (i) deleted the vertices where branches touch using ‘Select Vertices’ and ‘Delete Selected Vertices’ filters; (ii) removed duplicates and isolated vertices and faces using the filters ‘Remove Duplicated Vertex’, ‘Remove Duplicate Faces’, ‘Remove Isolated pieces (wrt Diameter)’, and ‘Remove Unreferenced Vertex’.

#### Geometric inflorescence architecture traits

We extracted 15 geometric traits from scanned inflorescences (Fig. 2; Supplementary Fig. S2). Detailed trait descriptions and calculations are explained in Supplementary Table S1. Trait illustrations, including examples of low and high values for each trait, are available in Fig. 2 and Supplementary Fig. S2. Traits were organized in one of three trait groups: global-size features, local-branching features, and size-invariant features (Table 2). PedicelDiameter and PedicelBranchAngle were measured using the software DynamicRoots (Symonova *et al.*, 2015) on a subset of detected pedicels from the raw 3D volume data. All other traits were derived from Matlab algorithms. Branch length traits (i.e. TotalBranchLength, RachisLength, PedicelLength, and AvgBranchLength) were derived from the persistence barcode (see next subsection).

#### Quantifying branching topology using persistent homology, a topological data analysis method

Persistent homology measures shapes based on a tailored mathematical function, such as geodesic distance, which we used here to capture both curved length and topology of the branches (Fig. 3; Supplementary Video S1). The geodesic distance of a point is the length of the shortest curve connecting the point and the base (e.g. purple curves, Fig. 3A), where the tailored base can be set as the first node or ground level (the brown line in Fig. 3A). For each branch, the tip always has the largest geodesic distance from the base (Fig. 3B). A level represents the collection of points whose geodesic distances are the same (e.g. geodesic distance=90, pink curve in Fig. 3A). A superlevel set, for example, at 90, is all the points whose geodesic distances are greater than 90 (black branch tips, Fig. 3A). Changing the level value from largest to smallest (x-axis, Fig. 3C), the sequence of nesting superlevel sets can be formed, which is named superlevel set filtration (top panel, Fig. 3C). During the change of the level value, bars record the connected components for each of the superlevel sets. When a new component arises, a new bar starts (e.g. at level 112, purple branch,

Fig. 3C). When two components merge (e.g. at level 65, orange branch merges into purple branch, Fig. 3C), the shorter bar stops (e.g. the orange bar stops at level 65, Fig. 3C). This bar graph, called the persistence barcode, summarizes topological information such as branching hierarchy, branch arrangement, and branch lengths. In our study, we set the base as the junction between peduncle and rachis (the lowermost node, indicated by a brown line in Fig. 1E and Fig. 3D, F) and use this base to compute the persistence barcode for the inflorescence architecture (Fig. 3E, G).

The persistence barcode can be used to compare topological similarity between any two inflorescences. To compute pairwise distance among persistence barcodes for the entire inflorescence population, we used the bottleneck distance (Cohen-Steiner *et al.*, 2007). Bottleneck distance is a robust metric that calculates the minimal cost to move bars from one persistence barcode to resemble another (Li *et al.*, 2017). We performed multidimensional scaling (MDS) on the pairwise bottleneck distance matrix and projected the data into lower dimensional Euclidean space by preserving the pairwise distance as well as possible. The Matlab (R2017a) MDS function cmdscale() projects the data so that MD1 acts as principal component (PC) 1 representing the most variation. The first three PCs (MDs) explained about 80% of the total variation and were included as traits: PersistentHomology\_PC1 (PH\_PC1, explained about 54% of the variation), PersistentHomology\_PC2 (PH\_PC2, explained about 20% of the variation), and PersistentHomology\_PC3 (PH\_PC3, explained about 6% of the variation). Those traits not only measure the topological structure, but also relate to geometric variation (e.g. global size) as the data were not normalized (Fig. 2; Supplementary Table S1).

Next, we normalized the persistence barcode by the TotalBranchLength (summation of the bar lengths) so that the TotalBranchLength was 1. By a similar procedure, we derived the first three PCs named PersistentHomologyNormalizedByTotalBranchLength\_PC1 (PHn\_PC1, explained about 45% of the variation), PersistentHomologyNormalizedByTotalBranchLength\_PC2 (PHn\_PC2, explained about 21% of the variation), and PersistentHomologyNormalizedByTotalBranchLength\_PC3 (PHn\_PC3, explained about 7% of the variation) for the normalized inflorescence topological structure (Fig. 2; Supplementary Table S1).

#### Berry potential, an approach to indirectly explore the space limited by inflorescence architecture

An ongoing question in grapevine cluster architecture is the relationship between inflorescence architecture and berry number and size. Inflorescence architecture is one of several factors determining the number of berries that can form, due to the number of pedicels and the available space for berry development. In this study, berries were removed because of concerns about berry integrity during transport from New York to Missouri, and the time between harvest and scanning. Instead

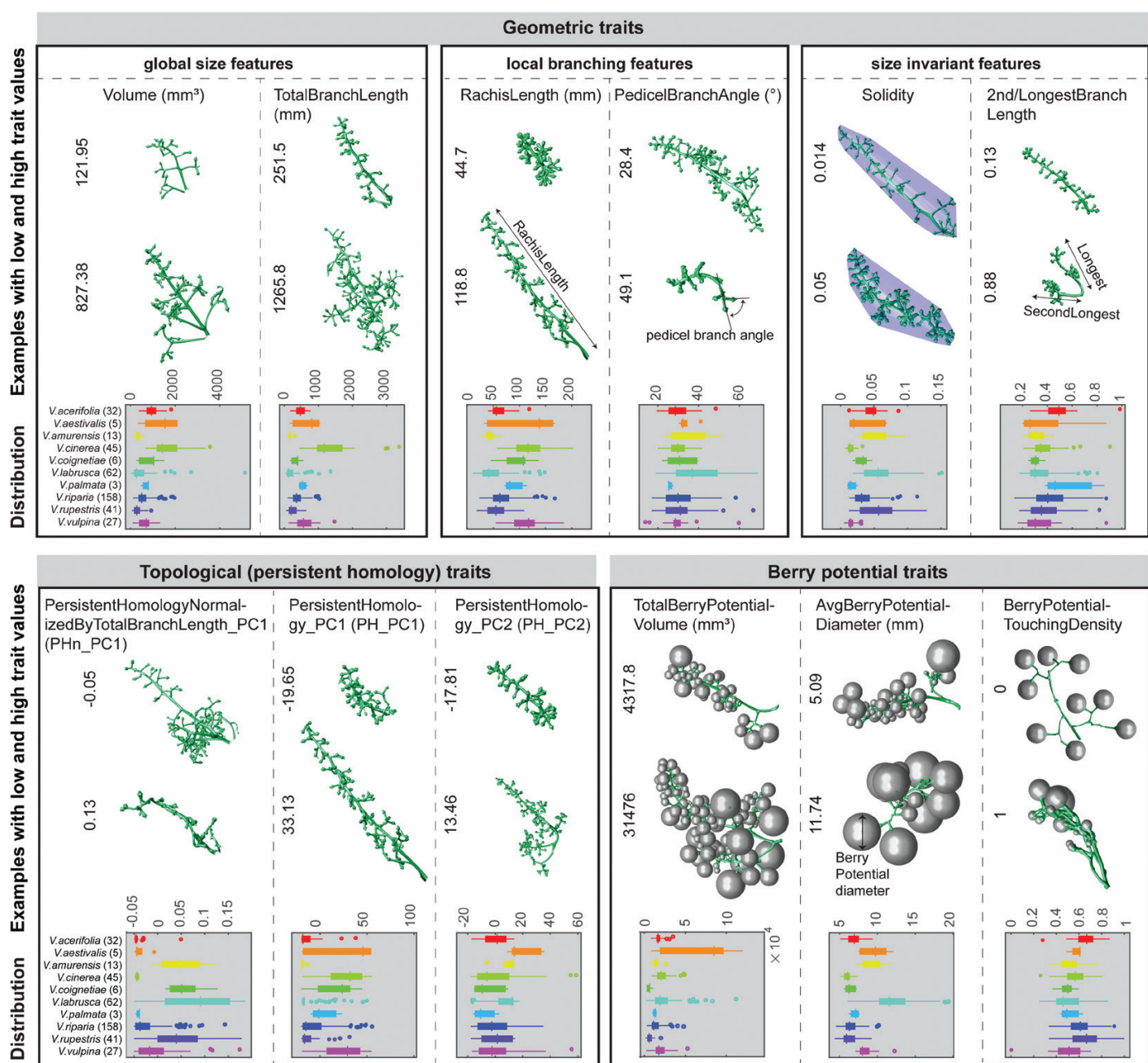


**Fig. 2.** Examples of inflorescence geometric and topological traits and their distribution for 10 *Vitis* species. Each panel shows one of the three traits categories (geometric traits, topological traits, and berry potential traits). Geometric traits are organized as global size features, local branching features, and size-invariant features. Each trait is listed at the top of the column and two inflorescence examples demonstrating low and high trait values listed to the left. At the bottom of each column is a boxplot indicating the distribution and variance within the 10 *Vitis* species, represented in different colors. On each box, each circle indicates an outlier if it is more than 1.5 interquartile ranges; the central vertical line indicates the median; the left and right edges of the box represent the 25th and 75th percentiles; and the whiskers extend to the most extreme non-outlier data. The label for each species is listed in the boxplot y-axis of the leftmost plot, with the number of individuals sampled for each species shown in parentheses. For a more complete example and detailed description of each trait, see Fig. S2 and Table S1.

of looking directly at berries on the cluster, we used inflorescence architecture as a starting point to simulate potential space available for berry growth by evaluating expanding spheres attached to pedicels. The extent of sphere expansion allowed by each pedicel is referred to as ‘berry potential’ (Fig. 4; Supplementary Video S2).

We first determined the growth direction for each berry potential based on the pedicel orientation. When spheres expand, the center moves along the pedicel direction (Fig. 4A). This step can be achieved by performing principal component analysis (PCA) on the near-berry segment of the pedicel. The first principal axis is the pedicel direction. We adjusted

the arrow of the direction to make sure berry potential increases outward along the pedicel orientation. Then the berry potential increases until one of three situations is encountered (Fig. 4B): (i) if two berry potentials touch each other, both berry potentials will stop increasing; (ii) if a berry potential touches any part of the inflorescence, it will stop increasing; (iii) if the diameter of the berry potential reaches the maximum size known for that species (Table 1), it will stop increasing. For each species, the maximum size is defined as the maximum berry diameter, a number estimated from known ranges of berry sizes for each species, based on values obtained from Galet (1988) and Moore and Wen (2016).

**Table 2.** Fifteen geometric traits were organized into three categories based on the type of shape information captured by the trait

Global-size features	Local-branching features	Size-invariant features
Volume <sup>a</sup>	RachisLength <sup>a</sup>	Solidity
ConvexHullVolume <sup>a</sup>	PedicelLength	Sphericity
SurfaceArea <sup>a</sup>	AvgBranchLength	2nd/LongestBranchLength
TotalBranchLength <sup>a</sup>	BranchDiameter	PedicelLength/RachisLength
NumberOfPedicel <sup>a</sup>	PedicelDiameter	
	PedicelBranchAngle	

See [Supplementary Table S1](#) for a more detailed description of each trait.  
<sup>a</sup> these features plus PH\_PC1 comprise 'Size-associated features'.

Berry potential does not reflect true berry growth; rather, berry potential is a derived attribute of inflorescence architecture, an indirect estimate of the space potentially available for berry growth. It also does not account for the possibility of branches bending or otherwise becoming reoriented due to pressure from growing berries. Berry potential is based on the number of neighbor pedicels, neighbor pedicel lengths, and neighbor pedicel mutual angles. Larger values for berry potential are associated with fewer neighbor pedicels and/or longer pedicel lengths and/or larger mutual angles. From the berry potential simulation, we calculated three features, TotalBerryPotentialVolume, AvgBerryPotentialDiameter, and BerryPotentialTouchingDensity, which is the berry potential touching number (i.e. touching either another berry potential or any part of the inflorescence) divided by the number of berry potential ([Fig. 2; Supplementary Table S1](#)).

To compare the berry potential with the true berry features, we XRT scanned 10 clusters with berries attached representing five commercially available table grape (*Vitis vinifera*) varieties. We computationally identified the berries and measured the total berry volume, average berry diameter, and touching density. We then computationally removed the berries and calculated the berry potential features based on the stalk. The linear regression ( $R^2=0.93, 0.99$ , and  $0.76$ , respectively) and normalized root mean square error (RMSEn=11, 3, and 14, respectively) indicate that berry potential provides a realistic model of actual grapevine cluster traits (see [Supplementary Fig. S3](#)). We note that the current simulation will better estimate relatively loose clusters with round berries than highly compact clusters in which berries touch, are deformed by pressing, and are not spherical. Our intent is to further parameterize the simulation by scanning even more diverse germplasm to incorporate a wider range of cluster architectures and berry traits in future work.

#### Phylogenetic analysis

Phylogenetic analyses were conducted to understand evolutionary trends in inflorescence architecture in *Vitis*. Single nucleotide polymorphism (SNP) markers were generated as part of a separate study of the USDA Grapevine Germplasm Reserve in Geneva, NY, USA ([Klein et al., 2018](#)). The original dataset consisted of 304 individuals representing 19 species that were sequenced using genotyping-by-sequencing (GBS; [Elshire et al., 2011](#)). Briefly, [Klein et al. \(2018\)](#) filtered data to retain biallelic sites with a minimum allele frequency of 0.01, a minimum mean depth of coverage of 10X, and only sites with <20% missing data and individuals with <20% missing data. We extracted SNP data for 99 of the individuals from this study that were also genotyped in [Klein et al. \(2018; Table 1\)](#) and performed phylogenetic analysis using SVDquartets ([Chifman & Kubatko, 2014](#)), a maximum likelihood approach designed to address ascertainment bias associated with reduced representation sequencing techniques like GBS. We analysed all possible quartets and carried out 100 bootstrap support runs (see [Supplementary Fig. S1](#)) using PAUP\* version 4.0a ([Swofford, 2003](#)). The three main clades recovered in the tree were consistent with previous phylogenetic work in *Vitis*: (i) an Asian clade (*V. amurensis* and *V. coignetiae*), (ii) North American clade I (*V. riparia*,

*V. acerifolia*, and *V. rupestris*), and (iii) North American clade II (*V. vulpina*, *V. cinerea*, *V. aestivalis*, *V. labrusca*, and *V. palmata*) ([Tröndle et al., 2010](#); [Zecca et al., 2012](#); [Miller et al., 2013](#); [Zhang et al., 2015](#); [Klein et al., 2018](#)).

To visualize trait distributions on a phylogenetic tree using branch lengths, we used Mega X ([Kumar et al., 2018](#)) to generate a neighbor joining tree with 2000 bootstrap replicates. All measurements were averaged across the three replicates per genotype to produce an average value for each trait for each genotype. We computed Pagel's lambda to estimate phylogenetic signal for each morphological trait and mapped each trait onto the phylogeny (see [Supplementary Fig. S4A–X](#)) using the R package phytools (v. 0.6–44; [Revell, 2012](#)). We calculated variation of each morphological trait for each clade based on the mean value for each species ([Supplementary Fig. S5](#)).

#### Statistical analysis

PCA, MDS, and hierarchical cluster analysis generating a hierarchical tree were performed in Matlab using functions pca(), cmdscale(), and clustergram(). The R function cor.mtest() and package corrplot ([Wei & Simko, 2017](#)) were used for significance tests and correlation matrix visualization. The function lda() in R package MASS ([Venables & Ripley, 2002](#)) was used for the linear discriminant analysis (LDA) with a jackknifed 'leave one out' cross validation method.

#### Code availability

All Matlab functions used to calculate persistence barcodes, bottleneck distances, simulation for berry potential, other geometric features used in this study, and the script for extracting phylogenetic information can be found at the following GitHub repository: <https://github.com/Topp-Roots-Lab/Grapevine-inflorescence-architecture>.

## Results

### Inflorescence morphological variation and trait correlation within *Vitis* species

We investigated 24 morphological traits (15 geometric traits, six PH traits, and three berry potential traits) of inflorescence architecture in 10 wild *Vitis* species (136 genotypes, 392 samples) and detected wide variation in morphological features within and between species ([Fig. 2; Supplementary Fig. S2; Supplementary Table S2](#)). In particular, of all the species examined, *V. aestivalis* had the largest variance for TotalBerryPotentialVolume. *Vitis labrusca* had the largest variance for 10 traits (i.e. pedicel features, Sphericity, AvgBranchDiameter, AvgBerryPotentialDiameter, and normalized topological traits). *Vitis cinerea* had the largest variance for six traits (i.e. most global-size features, PH\_PC2, and PH\_PC3). In comparison, *V. palmata* had the smallest variance for eight traits (i.e. pedicel features, Sphericity, AvgBranchDiameter, TotalBerryPotentialVolume, PH\_PC3, and PHn\_PC3), as did *V. amurensis* (global-size features, RachisLength, PH\_PC1, and PH\_PC2).

All traits were hierarchically clustered based on the mean trait values for each species, classifying traits into two main categories: mostly size-invariant+local-branching features (PHn\_PC3 to PedicelLength) versus global-size features (AvgBranchLength to BerryPotentialTouchingDensity) ([Fig. 5A](#)). Hierarchical clustering ([Fig. 5A](#)) and pairwise correlation for morphological traits ([Fig. 5B](#)) showed that global-size features (ConvexHullVolume, SurfaceArea, Volume, NumberOfPedicel, and TotalBranchLength), PH\_PC1, and RachisLength were all highly positively correlated. We refer

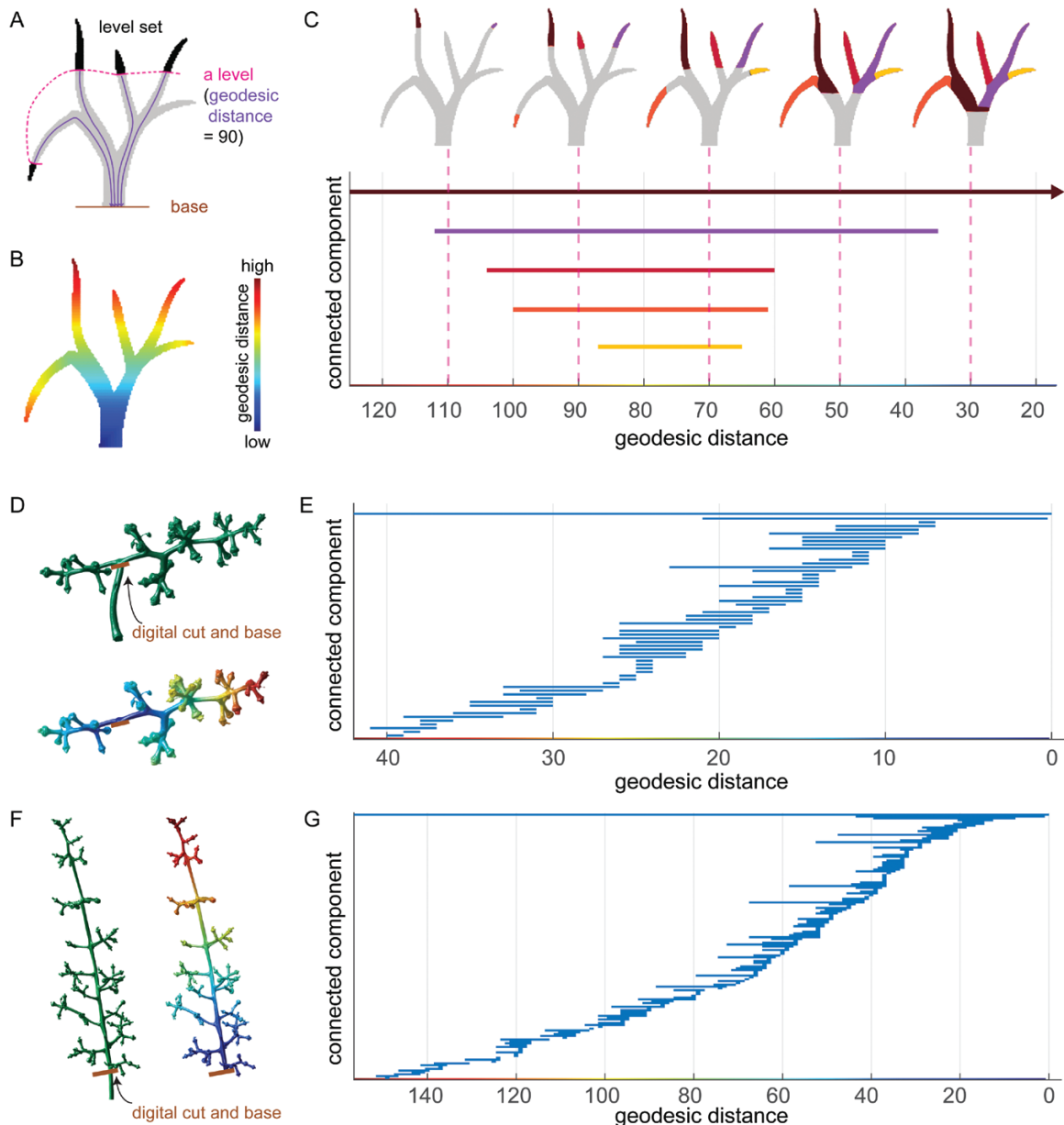


**Fig. 3.** Persistent homology with geodesic distance comprehensively quantifies branching structures. (A) A level (pink solid line) defined by the same geodesic distance (length of any of the purple curves, in this case, set to 90) to the base of the inflorescence. The super level set is the pixels (in black) having greater geodesic distance than the pink level. (B) Pixels on a branching structure are colored by their geodesic distance to the base. They are colored with red representing the most distant through to blue for the closest ones. (C) A persistence barcode for each branching structure records the connected components for each level set at each geodesic distance value. The ‘birth’ and ‘death’ values for each bar represent the level where each branch starts and gets merged. Colored bars correspond to colored branches. (D) Above: example inflorescence. The stem is digitally cut at the base (brown line) where it meets the first branch. Below: 3D surface on the example inflorescence as in (B). (E) Persistence barcode for the inflorescence in (D). (F, G) Similar to (D, E) showing a different inflorescence architecture.

to these seven traits as size-associated features. Size-associated features were negatively correlated with PedicelLength/RachisLength, Solidity, Sphericity, and PHn\_PC1. Some traits were relatively independent such as 2nd/LongestBranchLength, PedicelLength, PedicelBranchAngle, PH\_PC2, PHn\_PC2, and PHn\_PC3 (Fig. 5B). PHn\_PC3 had some negative relation with size-invariant features. PHn\_PC1 positively correlated with Sphericity, Solidity, and AvgeBerryPotentialDiameter (Fig. 5B). Pairwise correlations of morphological features (allometric relationships) for each of the species varied widely (Fig. 5C; for all traits see Supplementary Fig. S6A–X). For example, more

pedicels typically result in smaller berry potential diameters, except for *V. aestivalis*. Longer branches tended to be thinner, except for *V. coignetiae*, and correlate with larger inflorescences, except in *V. acerifolia*.

Hierarchical clustering of 10 *Vitis* species based on the 24 morphological traits resolved four groups: (i) *V. cinerea*, (ii) *V. aestivalis*, (iii) *V. coignetiae*–*V. vulpina*–*V. palmata*–*V. acerifolia*–*V. riparia*–*V. rupestris*, and (iv) *V. amurensis*–*V. labrusca* (Fig. 5A). Among the 10 *Vitis* species examined in this study, the largest variance in mean trait values were seen in *V. cinerea* (Fig. 5A). *Vitis cinerea* samples were generally larger than those from

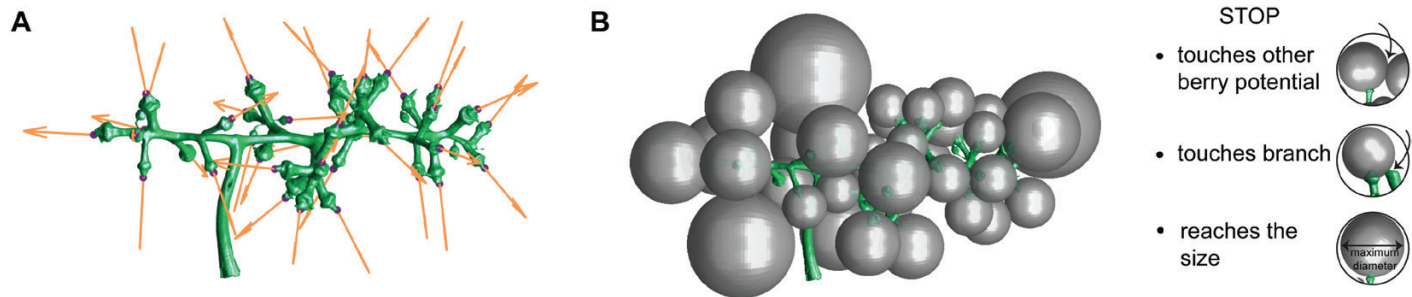


**Fig. 4.** Berry potential simulation to explore the space determined by inflorescence architecture. (A) Determine the growth direction for each berry potential. (B) Expand berry potential by increasing the size and moving the center along the growth direction until it meets any of these three cases: (i) two berry potentials touch each other; (ii) a berry potential touches any part of the inflorescence; (iii) the diameter of the berry potential reaches the maximum for the species.

the other species, as reflected in size-associated traits. Topology traits such as PHn\_PC3 and size-invariant traits like Sphericity and Solidity were lower in the mean trait value for *V. cinerea* than for other species. Similarly, mean trait values were larger for size-associated traits in *V. aestivalis* (Fig. 5A). Compared with other species, topology and berry potential traits were larger in *V. aestivalis*. Mean trait values of the third group (*V. coignetiae*–*V. vulpina*–*V. palmata*–*V. acerifolia*–*V. riparia*–*V. rupestris*, Fig. 5A) tended to be nearer to middle values compared with the other species. Within this group, *V. acerifolia*–*V. riparia*–*V. rupestris* typically were larger in the mean trait value for berry potential touching (i.e. denser berry potentials). These three species and *V. palmata* tend to have large, first primary branches (i.e. wings; Fig. 1E). *Vitis coignetiae* has thicker branches and *V. vulpina* has longer pedicels compared with other species in this group. The final group, *V. amurensis* and *V. labrusca*, have relatively smaller inflorescences with thicker branches compared with the other species sampled here. These general features are reflected in larger mean values for several size-invariant and local-branching features and smaller mean values for many branch length-dependent and size-associated features, respectively (Fig. 5A).

#### Multivariate, discriminant analysis of *Vitis* species based on inflorescence architecture

In order to understand how overall inflorescence architecture varies among *Vitis* species, we performed PCA using all 24 morphological features and all samples. PC1 explained 37.12% of the total variation in the measured architecture (Fig. 6A). The traits with the largest values for PC1 loadings, indicating that they contributed most to variation, were size-associated features, Solidity and Sphericity. PC2 explained 15.4% of the total variation in the measured inflorescence architecture, with variation primarily explained by local-branching features such as PedicalDiameter, PedicelLength, PedicelLength/RachisLength, AvgBranchLength, BranchDiameter, three berry potential traits, and PHn\_PC1 (Fig. 6A). Although inflorescences from each species occupy different regions of morphospace, these regions overlap considerably.

LDA performed on the first 18 PCs explaining 99.5% of the variation, distinguished between species with a classification accuracy rate of 78.32%. A confusion matrix (Fig. 6B)

shows the proportion of samples correctly predicted for each species. LD1 primarily separates *V. cinerea*, *V. labrusca*, and *V. amurensis* from the other species while LD2 primarily separates *V. vulpina* and *V. coignetiae*. The traits that are most important for distinguishing these species, as indicated by LD loadings, are TotalBerryPotentialVolume and PHn\_PC1 for LD1, and AvgBranchLength and AvgBerryPotentialDiameter for LD2 (Fig. 6B). The most important predictors for correctly separating any two species are shown as the grey scaled boxes in Supplementary Fig. S7 and Table S3. For example, BranchDiameter and PedicelDiameter are key when contrasting *V. coignetiae* and *V. vulpina*, suggesting that different branch thickness easily distinguishes these two species. This method correctly determined species classifications with 100% accuracy when contrasting *V. aestivalis* and *V. cinerea*, *V. aestivalis* and *V. palmata*, *V. aestivalis* and *V. vulpina*, *V. amurensis* and *V. cinerea*, *V. amurensis* and *V. palmata*, *V. cinerea* and *V. coignetiae*. Other combinations of species are harder to distinguish on the basis of inflorescence characters. For example, the classification accuracy rate was only 80% when distinguishing between *V. amurensis* and *V. labrusca* and 82% for *V. aestivalis* and *V. coignetiae*.

#### Phylogenetic signal of inflorescence architecture within clades

The phylogeny dataset ( $n=99$ ) is generally well-supported at the species level and correlates well with current taxonomy. Using average trait values per individual, Pagel's lambda showed 12 morphological traits (seven size-associated features along with PedicelDiameter, TotalBerryPotentialVolume, Sphericity, PH\_PC2, PHn\_PC1) have a strong phylogenetic signal ( $\lambda > 0.8$ ; Fig. 7; Supplementary Table S4). While most species sampled tended to have small values for the seven size-associated features, *V. aestivalis*, *V. cinerea*, and *V. vulpina* tended to have values that were either close to median or larger. On average, *V. labrusca* had larger values for Sphericity and PHn\_PC1 compared with other species sampled, while *V. cinerea* generally had some of the smallest values for these traits. Only two morphological traits (2nd/LongBranchLength,  $\lambda = 0.06$  and BerryPotentialTouchingDensity,  $\lambda = 0.25$ ) lacked phylogenetic signal (Fig. 7; Supplementary Table S4).

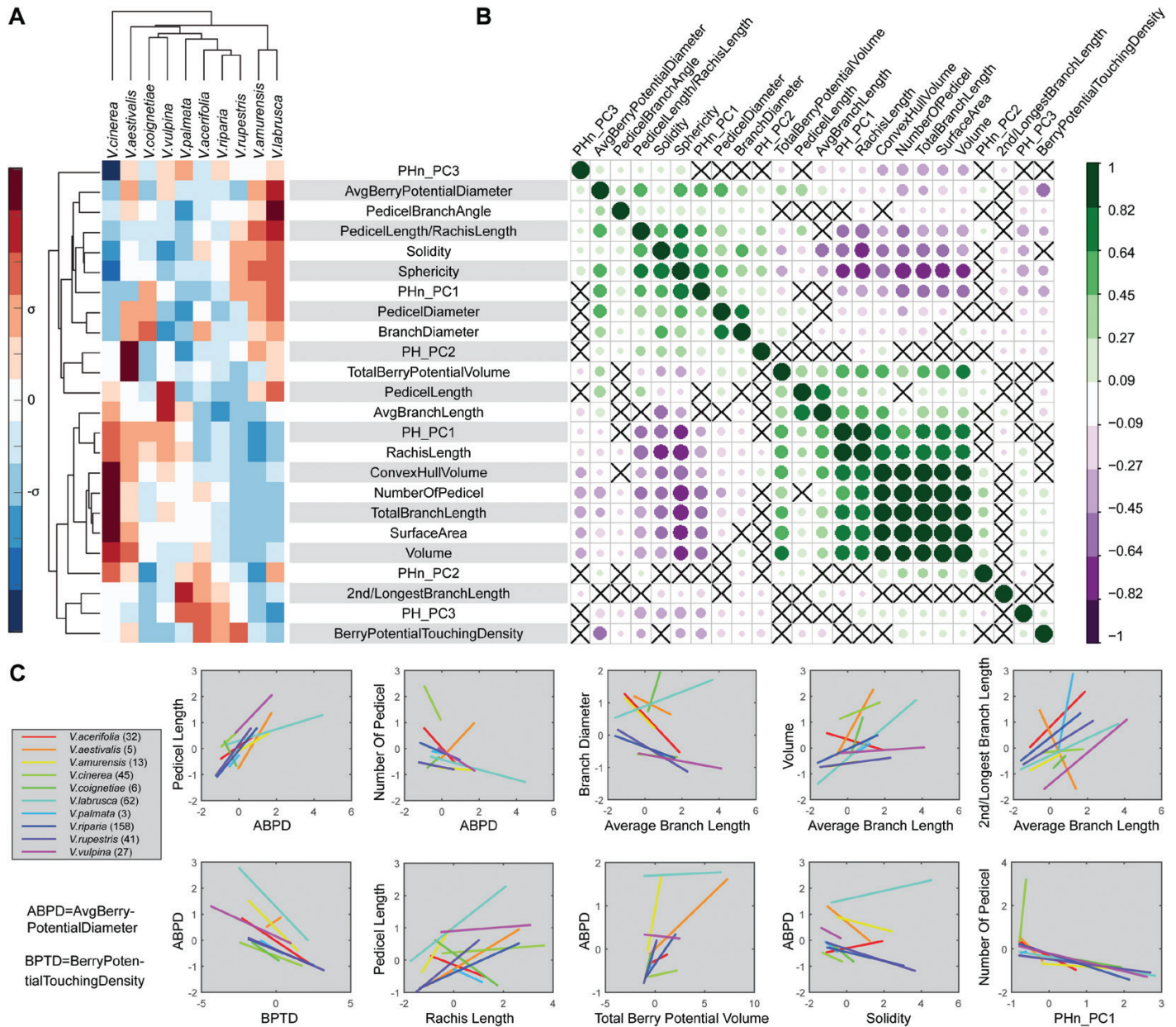


**Fig. 5.** Hierarchical cluster analysis and correlation analysis. (A) Cluster analysis based the mean value for each trait of 10 *Vitis* species. The heatmap shows values above (red) or below (blue) the mean for each trait. The morphological traits (rows) are clustered hierarchically with the name shown on the right and hierarchical tree listed on the left. The species (columns) are also clustered hierarchically with the name and hierarchical tree shown at the top. (B) Correlation matrix plot shows pairwise positively stronger correlation (green and larger circle) or negatively stronger correlation (purple and larger circle). Non-significant correlations ( $P > 0.05$ ) are crossed out. The traits are ordered in the same way as in (A). (C) Selected pairs of traits showing linear regression lines for each species.

We observed differences in *Vitis* inflorescence architecture among clades and between species. For North American (NA) clade I (*V. acerifolia*, *V. riparia*, *V. rupestris*), variation in the 24 morphological traits measured had similarly small values among species, particularly for several size-associated traits, although there was relatively large variation for PHn\_PC3 and BerryPotentialTouchingDensity (Fig. 7). Within NA clade I, we observed differences among clade members for traits such as Sphericity and PHn\_PC1 (larger in *V. rupestris* compared with other clade members) and PedicelDiameter and BranchDiameter (slightly larger in *V. acerifolia* compared with

other clade members; Fig. 7). NA clade II appeared to be more variable among clade members. *Vitis cinerea* had larger values for size-associated traits compared with clade members *V. labrusca*, *V. palmita*, and *V. vulpina*. Meanwhile, *V. labrusca* typically had larger values for local features (e.g. Sphericity, PedicelDiameter, AvgBerryPotentialDiameter, PedicelBranchAngle) compared with the other clade members (Fig. 7).

We calculated the mean value for each species of each morphological trait to study variation within the three clades and detect subtle signatures (Fig. 7). We computed the variance for the multivariate trait (combining all the 24 traits), and each

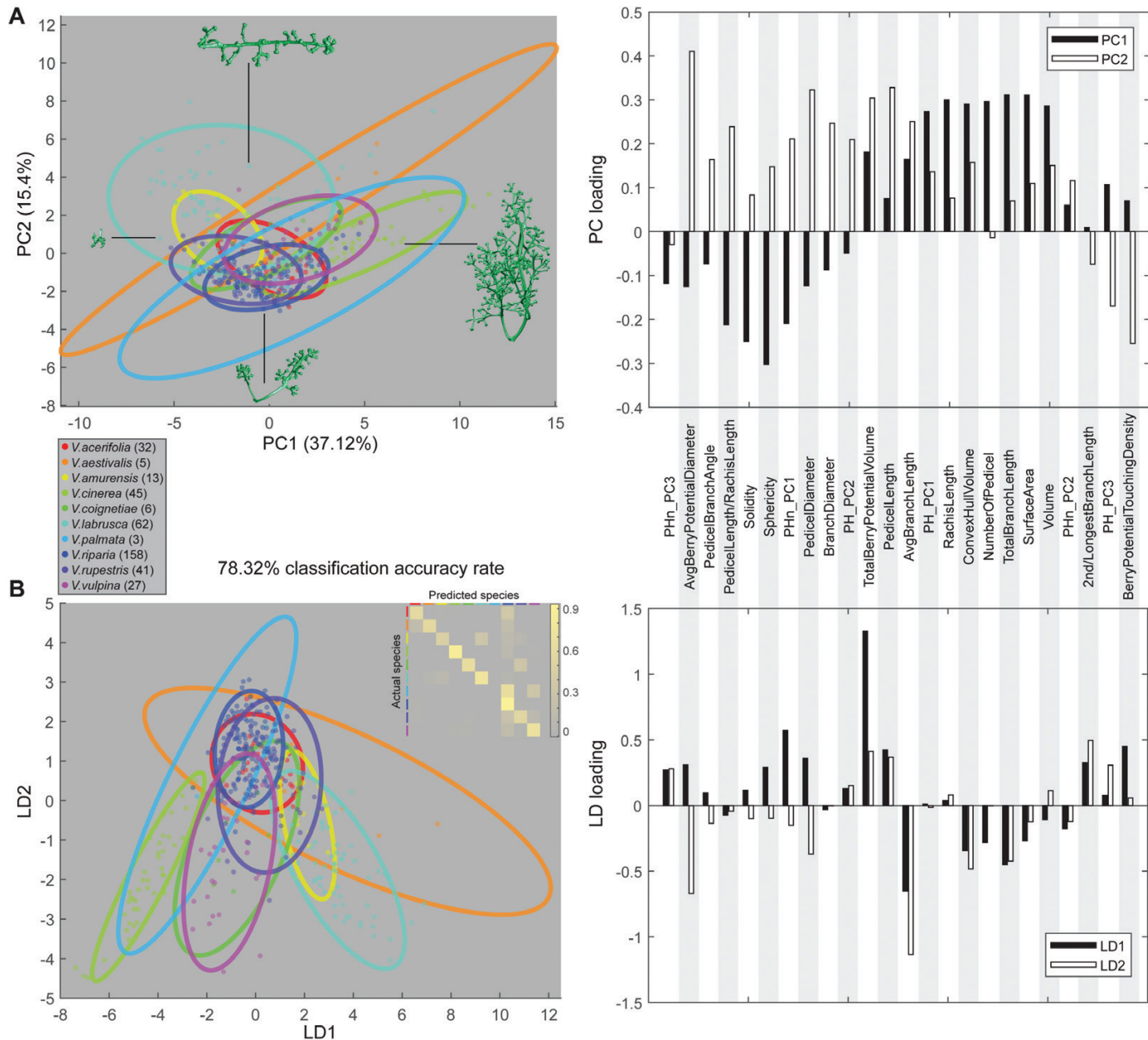


**Fig. 6.** Classification for 10 *Vitis* species based on inflorescence architecture. (A) Left: principal component analysis (PCA) plot on 24 morphological traits. The percent variance for each PC explained is shown in parentheses. Species are shown in different colors. Right: the loadings for the traits that contribute to the variance are shown. (B) Left: linear discriminant analysis (LDA) plot on the first 18 PCs (99.5% variance). Species are shown in different colors. The confusion matrix for predicted species is shown in the upper right corner. Right: the loadings for the traits that best distinguish species from each other. Using a jackknifed ‘leave one out’ cross validation, we obtain a 78.32% classification accuracy rate.

of these 24 traits for each clade (see [Supplementary Fig. S5](#); [Supplementary Table S5](#)). Overall, based on the samples used in this analysis, variance of the multivariate trait for NA clade I (variation=0.14) was much smaller than that for NA clade II (variation=0.64), while the variation for the Asian clade was 0.39. Some traits had almost no variance in the Asian clade such as PedicelDiameter, PHn\_PC2, PHn\_PC3, and 2nd/LongestBranchLength. However, North American species (8/~19 taxa) in this study were better represented than Asian species (2/~37 taxa), so we are cautious not to over-interpret this finding. Traits with the greatest variance in the Asian

clade included PedicelLength/RachisLength, RachisLength, and PHn\_PC1, while NA clade I had the greatest variance in PHn\_PC2. All the other traits had greatest variance in NA clade II ([Supplementary Fig. S5](#), [Supplementary Table S5](#)). Traits with the smallest variance in the Asian clade included PHn\_PC3, PHn\_PC1, PedicelDiameter, BranchDiameter, NumberOfPedicel, 2nd/LongestBranchLength, PHn\_PC3, and BerryPotentialTouchingDensity. The other traits had small variance in NA clade I ([Supplementary Fig. S5](#), [Supplementary Table S5](#)). Our results highlight clade-specific variation in inflorescence architecture for previously undescribed traits.

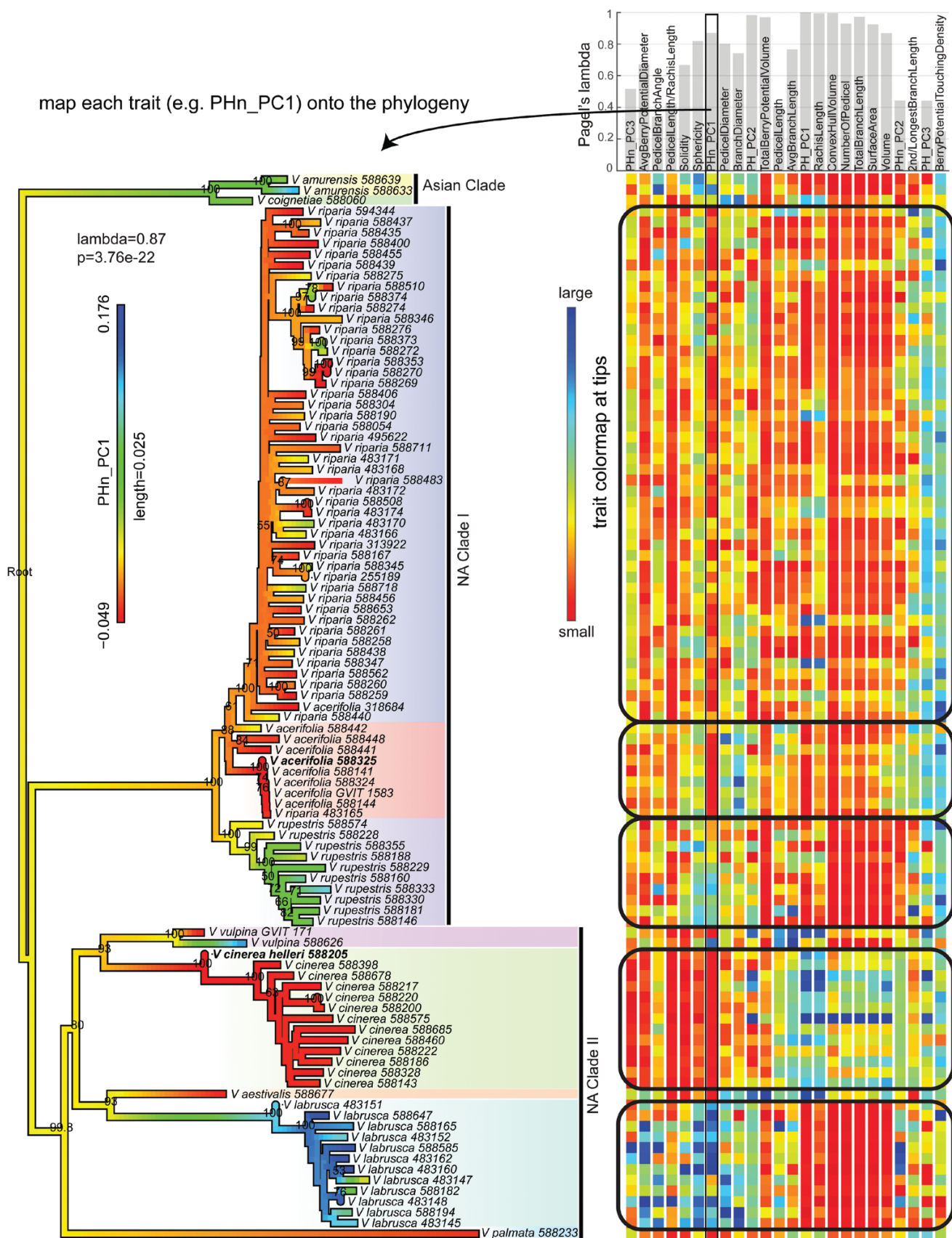


**Fig. 7.** Phylogenetic analysis. A neighbor joining phylogenetic tree for a subset of the *Vitis* dataset ( $n=99$ ). Node values denote bootstrap support for values  $\geq 50$ . Ten *Vitis* species are highlighted in different colored backgrounds. Three clades (Asian clade, NA clade I, and NA clade II) are labeled and marked by vertical bars. The barplot showing values of Pagel's lambda, an estimate of phylogenetic signal, overlaps with the trait name on the right top panel. Below each trait, a rainbow colormap shows the values for individuals (small values in red to large values in blue). Rectangles surround the trait value map for species with more than five individuals. One trait (PHn\_PC1) was randomly selected to be projected onto the phylogenetic tree branches, and indicates trait variation (red, lower values; blue, higher values) within individuals and among clades.

## Discussion

*X-ray imaging and advanced morphometrics is a powerful combination for characterizing complex phenotypes*

Inflorescence architecture has a strong influence on flower and fruit production and is therefore a trait of great scientific interest. Studies extend into interspecific variation, pollen dispersal, genetic architecture, evolution, regulation, and development of inflorescence structures (e.g. Bradley *et al.*, 1996; Friedman & Harder, 2004; Kellogg, 2007; Morris *et al.*, 2013; Han *et al.*, 2014; Hodge & Kellogg, 2015; Whipple, 2017; Stitzer & Ross-Ibarra, 2018; Ta *et al.*, 2018; Richter *et al.*, 2019). Yet the challenge remains to analyse these complex 3D branching structures with appropriate tools. High resolution datasets are required to represent the actual structure and comprehensive analysis of both the geometric and topological features relevant to phenotypic variation and to clarify evolutionary and developmental inflorescence patterns.

Our results demonstrate the power and potential of X-ray imaging and advanced morphometric analysis for investigating complex 3D phenotypic features. We analysed the phenotypic variation in inflorescence architecture of 10 wild *Vitis* species using computer vision and an emerging biological shape analysis method, persistent homology, which allowed comprehensive comparisons of shape. Although samples analysed here represent only a subset of the known variation in *Vitis*, which includes an estimated 60 species, our analyses demonstrate significant variation within and among *Vitis* species and among clades. Correlation analysis (Fig. 5B) revealed some unexpected relationships, for example pedicel branch angles were largely independent of other traits. It also shows that PH features are complementary, as they are relatively independent from most geometric features. We were able to assign widely differing architectures to biological species with high accuracy (Fig. 6) from the 24 different morphometric traits surveyed in this study. PH provides an important contribution to this discriminatory power, as does berry potential (Fig. 6B). We observed that traits such as the rachis length, the sum of all branches, the space encompassing the inflorescence architecture (ConvexHullVolume), and PH features can be indicative of species and clade (Fig. 7). Our results suggest meaningful, comprehensive information about the inflorescence structure was captured with a single measure (i.e. the persistence barcode) and that PH is a valuable method for quantifying and summarizing topological information.

Persistent homology analysis has led to a deeper understanding of trait genetic variation and architecture in plants (Li *et al.* 2018a,b). In grapevine, quantitative trait locus (QTL) analysis indicates a genetic basis to inflorescence architecture and berry compactness (Correa *et al.*, 2014; Richter *et al.*, 2019). Deploying PH-based topological modeling to grapevine mapping populations could lead to the rapid identification of additional inflorescence trait QTLs for breeding. For example, we observed total branch length (a proxy for bigger or smaller clusters) correlates with number of pedicels (a proxy for berry number; Fig. 5), an informative relationship to assess potential

yield. However, selecting for total branch length might lead to a negative correlation with the average berry potential diameter (i.e. smaller berries). Although this correlation may be desirable for wine grapes, it is not for table grapes.

### Linking complex phenotypes with evolutionary patterns to facilitate precision breeding

Grapevine cluster architecture is a composite feature that reflects multiple subtraits including stalk traits (inflorescence architecture) and berry features (Richter *et al.*, 2019). OIV 204 uses ‘bunch: density’ to describe variation in clusters, ranging from 1, berries clearly separated with many visible pedicels, to 9, berries deformed by compression (OIV, 2001; Rombough, 2002). Other authors have deconstructed traits contributing to cluster architecture primarily through individual measurements collected manually (e.g. Shavrukov *et al.*, 2004; Tello *et al.*, 2015; Zdunić *et al.*, 2015; Tello & Ibáñez, 2018) and more recently, with image-based technologies (Cubero *et al.*, 2014; Roscher *et al.*, 2014; Ivorra *et al.*, 2015; Aquino *et al.*, 2017, 2018; Rist *et al.*, 2018). Here, we were able to describe traits of interest that contribute greatly to the morphological features captured by the OIV scale (e.g. NumberOfPedicel, PedicelLength, PedicelBranchAngle, RachisLength, overall shape using PH; Fig. 2; Supplementary Fig. S2). This method could facilitate precision breeding for both whole inflorescence structure topology and specific desirable geometric traits.

While several studies have quantified cluster structure in cultivated grapevines, similar studies of wild *Vitis* inflorescence architecture are lacking. Munson (1909) and Galet (1979) describe North American *Vitis* cluster structure qualitatively, commenting on compactness, size, shape, and the presence of large first primary branches (wings/shoulders). Taxonomic descriptions typically do not examine inflorescence architecture beyond categorical type, position on the vine, and the average number of berries per cluster (Comeaux *et al.*, 1987; Moore, 1991; Moore & Wen, 2016). Descriptions of the position of the inflorescence are useful for identification and are included in dichotomous keys; however, to our knowledge, other inflorescence architecture traits have not been rigorously quantified among wild *Vitis* species. Although qualitative descriptions are valuable and accessible, powerful phenotyping tools are required to associate complex phenotypes with evolutionary and developmental patterns.

Using 3D imaging and PH with a topological modeling approach, we identified attributes of inflorescence architecture that vary within and among *Vitis* species that, to our knowledge, have not been previously described. Differences in inflorescence architecture among clades mirror other phenotypic differences among members of North American *Vitis*. For example, members of NA clade I (*V. acerifolia*, *V. riparia*, and *V. rupestris*) have small values for size-associated features (e.g. RachisLength, ConvexHullVolume, NumberOfPedicel, TotalBranchLength, SurfaceArea, Volume) and relatively large values for PH\_PC3 and BerryPotentialTouchingDensity (Fig. 7). These species share suites of other morphological characters (nodal diaphragm, branch and leaf surface traits, and large

stipules; Moore 1991, Moore and Wen 2016, Klein *et al.*, 2018). It is possible that among closely related species conserved pathways generate vegetative and reproductive similarities.

Sample size is low for the Asian clade and most of NA clade II, limiting our ability to assess variation in these species; however, members of NA clade II do not have suites of shared inflorescence traits (*V. aestivalis*, *V. cinerea*, *V. labrusca*, *V. vulpina*; Klein *et al.*, 2018). Rather, *V. labrusca* has very small values for size-associated traits and larger values for local features compared with the other clade members, whereas *V. cinerea* has larger values for size-associated features and smaller values for local features (Fig. 7). This is consistent with the observation that aside from core phenotypic synapomorphies in the genus (tendril, bark, lenticel, and nodal diaphragm characters), members of NA clade IIb (*V. aestivalis*, *V. cinerea*, *V. labrusca*, and *V. vulpina*) do not share morphological traits unique to the clade (Klein *et al.*, 2018). These species mostly co-occur across their distributions (Callen *et al.*, 2016) and additional sampling of *Vitis* taxa is necessary to further explore these complex evolutionary patterns. We observed *V. amurensis* grouping with *V. labrusca* and *V. coignetiae* grouping with North American species in hierarchical cluster analysis (Fig. 5A). The former two species have relatively smaller inflorescence architectures with thicker branches compared with the other species sampled here. Taxonomic relationships among North American and Asian *Vitis* species have been historically challenging, with clades comprising species with disjunct distributions (Mullins *et al.*, 1992). Since current taxonomy resolves separate Asian and North American clades (Klein *et al.*, 2018), morphological similarity between these species likely reflects convergent evolution.

### Future directions

Three-dimensional imaging through XRT and advanced mathematical approaches like persistent homology provide new ways to visualize and interpret complex biological structures including inflorescences, and to understand the genetic and environmental factors underlying variation in their architecture. In grapevines, cluster density is an important trait that is used to assess grapevine crop quality and to forecast yield, in part because of the association between bunch density and fungal infestations such as *Botrytis* (Hed *et al.*, 2009; Iland *et al.*, 2011; Molitor & Beyer, 2014; Molitor *et al.*, 2018). This study expands on previous work identifying variation in inflorescence architecture among cultivars (Shavrukov *et al.*, 2004), finding notable differences in cluster architecture among species. A logical next step may be to use 3D images and PH with topological modeling to trace the development of inflorescences across multiple growing seasons in a mapping population. Methods presented here are also amenable to scanning with berries, provided some noteworthy technical challenges are first addressed (e.g. minimizing berry damage and rotting during transportation, cluster stabilization during scanning, and segmentation of 3D volumes with features that vary widely in their X-ray absorbance). This work would provide a more complete representation of cluster structure, as well as inform our berry potential simulation with genotype-specific

empirical data. We plan to develop predictive structural models of grapevine cluster development using these techniques.

Imaging and shape analysis approaches presented here can also be used to tease apart subtle environmental influences on inflorescence architecture, and the major agronomic trait of bunch density. Identifying environmental effects on phenotypic variation has important implications both for vineyard management and the assessment of intra-clone variation across geographic space. Cluster compactness can be manipulated through a variety of agronomic practices (Molitor *et al.* 2012; Gil *et al.* 2013; Frioni *et al.* 2017; Gourieroux *et al.* 2017; Poni *et al.* 2018; Reeve *et al.* 2018). Techniques described here can be used to quantify influences of specific treatments on cluster architecture. In addition, because grapevines are clonally propagated, clusters from the same widespread clones can be collected from different geographic locations, scanned, and analysed for variation. High resolution assessment of inflorescence architecture offers important insights into natural variation in bunch density and the genetic and environmental factors that influence it. The capacity to capture 3D variation in this complex trait over space and time represents a promising advance for a valuable potential target of selection in one of the most economically important berry crops in the world.

### Supplementary data

Supplementary data are available at JXB online.

Fig. S1. A maximum likelihood phylogenetic tree for 10 *Vitis* species.

Fig. S2. Summary of inflorescence geometric and topological traits and the distribution for 10 *Vitis* species.

Fig. S3. Comparison between X-ray scanned and simulated berry features for five commercially available table grape varieties.

Fig. S4. A neighbor joining phylogenetic tree for a subset of the *Vitis* dataset.

Fig. S5. Variation for each clade.

Fig. S6. Pairwise correlations of morphological traits (allometric relationships) showing linear regression lines for each species.

Fig. S7. Pairwise species classification.

Table S1. Trait description and calculation.

Table S2. Trait variance for each species.

Table S3. Trait loadings for two species classification.

Table S4. Trait Pagel's lambda for phylogenetic analysis.

Table S5. Trait variation for each clade.

Video S1. Illustration of quantifying branching topology using persistent homology.

Video S2. Berry potential simulation.

### Acknowledgements

The authors would like to acknowledge Elizabeth A. Kellogg (DDPSC) for valuable comments, particularly on phylogenetic analysis and inflorescence anatomy. We thank Noah Fahlgren (DDPSC) for computational assistance and Kari Miller (Washington University) for scanning assistance. We thank Zoë Migicovsky (Dalhousie University) for valuable

comments. This work was supported by funding from the United States National Science Foundation projects IIA-1355406 and IOS-1638507 to CNT, and DBI-1759796 to AJM.

## Author contributions

CNT, DHC, and JL designed the research; JL collected the samples and consulted on the biology; KD generated the X-ray data; LLK and AJM provided phylogenetic data and consulted for the biology; NJ and ML extracted pedicel diameter and angle; ML developed and extracted all the traits and conducted all the analysis and figures; ML, LLK, KD, JL, AJM, and CNT wrote the manuscript.

## References

- Aquino A, Barrio I, Diago M-P, Millán B, Tardaguila J.** 2018. vitisBerry: An Android-smartphone application to early evaluate the number of grapevine berries by means of image analysis. Computers and Electronics in Agriculture **148**, 19–28.
- Aquino A, Diago MP, Millán B, Tardaguila J.** 2017. A new methodology for estimating the grapevine-berry number per cluster using image analysis. Biosystems Engineering **156**, 80–95.
- Bettiga LJ.** 2003. Wine grape varieties in California. Oakland, CA, USA: University of California, Agricultural and Natural Resources Publications.
- Bioletti F.** 1938. Outline of ampelography for the vinifera grapes in California. Hilgardia **11**, 227–293.
- Bradley D, Carpenter R, Copsey L, Vincent C, Rothstein S, Coen E.** 1996. Control of inflorescence architecture in *Antirrhinum*. Nature **379**, 791–797.
- Brereton NJB, Ahmed F, Sykes D, Ray MJ, Shield I, Karp A, Murphy RJ.** 2015. X-ray micro-computed tomography in willow reveals tissue patterning of reaction wood and delay in programmed cell death. BMC Plant Biology **15**, 83.
- Bucksch A, Atta-Boateng A, Azihou AF, et al.** 2017. Morphological plant modeling: unleashing geometric and topological potential within the plant sciences. Frontiers in Plant Science **8**, 900.
- Callen ST, Klein LL, Miller AJ.** 2016. Climatic niche characterization of 13 North American *Vitis* species. American Journal of Enology and Viticulture **67**, 339–349.
- Chanderbali AS, Berger BA, Howarth DG, Soltis PS, Soltis DE.** 2016. Evolving ideas on the origin and evolution of flowers: new perspectives in the genomic era. Genetics **202**, 1255–1265.
- Chifman J, Kubatko L.** 2014. Quartet inference from SNP data under the coalescent model. Bioinformatics **30**, 3317–3324.
- Cignoni P, Callieri M, Corsini M, Dellepiane M, Ganovelli F, Ranzuglia G.** 2008. Meshlab: an open-source mesh processing tool. In: Scarano V, De Chiara R, Erra U, eds. Eurographics Italian Chapter Conference. Aire-la-Ville, Switzerland: The Eurographics Association, 129–136.
- Cohen-Steiner D, Edelsbrunner H, Harer J.** 2007. Stability of persistence diagrams. Discrete & Computational Geometry **37**, 103–120.
- Comeaux BL, Nesbitt WB, Fantz PR.** 1987. Taxonomy of the native grapes of North Carolina. Castanea **52**, 197–215.
- Coombe BG.** 1995. Adoption of a system for identifying grapevine growth stages. Australian Journal of Grape and Wine Research **1**, 100–110.
- Correa J, Mamani M, Muñoz-Espinoza C, Laborie D, Muñoz C, Pinto M, Hinrichsen P.** 2014. Heritability and identification of QTLs and underlying candidate genes associated with the architecture of the grapevine cluster (*Vitis vinifera* L.). Theoretical and Applied Genetics **127**, 1143–1162.
- Cubero S, Diago MP, Blasco J, Tardaguila J, Millán B, Aleixos N.** 2014. A new method for pedicel/peduncle detection and size assessment of grapevine berries and other fruits by image analysis. Biosystems Engineering **117**, 62–72.
- Delory BM, Li M, Topp CN, Lobet G.** 2018. archiDART v3.0: a new data analysis pipeline allowing the topological analysis of plant root systems. F1000 Research **7**, 22.
- de Ribou S de B, Douam F, Hamant O, Frohlich MW, Negruțiu I.** 2013. Plant science and agricultural productivity: why are we hitting the yield ceiling? Plant Science **210**, 159–176.
- Doebley J, Stec A, Hubbard L.** 1997. The evolution of apical dominance in maize. Nature **386**, 485–488.
- Earles JM, Knipfer T, Tixier A, Orozco J, Reyes C, Zwieniecki MA, Brodersen CR, McElrone AJ.** 2018. In vivo quantification of plant starch reserves at micrometer resolution using X-ray microCT imaging and machine learning. New Phytologist **218**, 1260–1269.
- Edelsbrunner H, Morozov D.** 2013. Persistent homology: theory and practice. In: Proceedings of the European Congress of Mathematics. Zürich: European Mathematical Society, 31–50.
- Elshire RJ, Glaubitz JC, Sun Q, Poland JA, Kawamoto K, Buckler ES, Mitchell SE.** 2011. A robust, simple genotyping-by-sequencing (GBS) approach for high diversity species. PLoS One **6**, e19379.
- Endress PK.** 2010. Disentangling confusions in inflorescence morphology: patterns and diversity of reproductive shoot ramification in angiosperms. Journal of Systematics and Evolution **48**, 225–239.
- Feng C-M, Xiang Q-YJ, Franks RG.** 2011. Phylogeny-based developmental analyses illuminate evolution of inflorescence architectures in dogwoods (*Cornus* s. l., Cornaceae). New Phytologist **191**, 850–869.
- Friedman J, Harder LD.** 2004. Inflorescence architecture and wind pollination in six grass species. Functional Ecology **18**, 851–860.
- Frioni T, Zhuang S, Palliotti A, Sivilotti P, Falchi R, Sabbatini P.** 2017. Leaf removal and cluster thinning efficiencies are highly modulated by environmental conditions in cool climate viticulture. American Journal of Enology and Viticulture **68**, 325–335.
- Galet P.** 1979. A practical ampelography. Ithaca, NY, USA: Cornell University Press.
- Galet P.** 1988. Cépages et Vignobles de France. Tome I: Les Vignes Américaines. Montpellier: Imprimerie Déhan.
- Gil M, Esteruelas M, González E, Kontoudakis N, Jiménez J, Fort F, Canals JM, Hermosín-Gutiérrez I, Zamora F.** 2013. Effect of two different treatments for reducing grape yield in *Vitis vinifera* cv Syrah on wine composition and quality: berry thinning versus cluster thinning. Journal of Agricultural and Food Chemistry **61**, 4968–4978.
- Godin C, Caraglio Y.** 1998. A multiscale model of plant topological structures. Journal of Theoretical Biology **191**, 1–46.
- Godin C, Costes E, Sinoquet H.** 1999. A method for describing plant architecture which integrates topology and geometry. Annals of Botany **84**, 343–357.
- Gomez FE, Carvalho G Jr, Shi F, Muliana AH, Rooney WL.** 2018. High throughput phenotyping of morpho-anatomical stem properties using X-ray computed tomography in sorghum. Plant Methods **14**, 59.
- Gourieroux AM, Holzapfel BP, McCully ME, Scollary GR, Rogiers SY.** 2017. Vascular development of the grapevine (*Vitis vinifera* L.) inflorescence rachis in response to flower number, plant growth regulators and defoliation. Journal of Plant Research **130**, 873–883.
- Guédron Y, Barthélémy D, Caraglio Y, Costes E.** 2001. Pattern analysis in branching and axillary flowering sequences. Journal of Theoretical Biology **212**, 481–520.
- Hake S.** 2008. Inflorescence architecture: the transition from branches to flowers. Current Biology **18**, R1106–R1108.
- Han Y, Yang H, Jiao Y.** 2014. Regulation of inflorescence architecture by cytokinins. Frontiers in Plant Science **5**, 669.
- Haus MJ, Li M, Chitwood DH, Jacobs TW.** 2018. Long-distance and trans-generational stomatal patterning by CO<sub>2</sub> across *Arabidopsis* organs. Frontiers in Plant Science **9**, 1714.
- Hed B, Ngugi HK, Travis JW.** 2009. Relationship between cluster compactness and bunch rot in Vignoles grapes. Plant Disease **93**, 1195–1201.
- Hertweck KL, Pires JC.** 2014. Systematics and evolution of inflorescence structure in the *Tradescantia* alliance (Commelinaceae). Systematic Botany **39**, 105–116.
- Hodel DR, Greby K, Ohara LM, Ohara ET.** 2015. Inflorescence and fruit characteristics of *Washingtonia* (Arecaceae: Coryphoideae). Palm Arbor **2**, 1–7.
- Hodge JG, Kellogg EA.** 2015. Patterns of inflorescence development of three prairie grasses (Andropogoneae, Poaceae). International Journal of Plant Sciences **175**, 963–974.

- Hughes N, Askew K, Scotson CP, Williams K, Sauze C, Corke F, Doonan JH, Nibau C.** 2017. Non-destructive, high-content analysis of wheat grain traits using X-ray micro computed tomography. *Plant Methods* **13**, 76.
- Iland P, Dry P, Proffitt T, Tyerman S.** 2011. The grapevine: from the science to the practice of growing vines for wine. Adelaide, Australia: Patrick Iland Wine Promotions.
- Ivorra E, Sánchez AJ, Camarasa JG, Diago MP, Tardaguila J.** 2015. Assessment of grape cluster yield components based on 3D descriptors using stereo vision. *Food Control* **50**, 273–282.
- Jhala VM, Thaker VS.** 2015. X-ray computed tomography to study rice (*Oryza sativa* L.) panicle development. *Journal of Experimental Botany* **66**, 6819–6825.
- Kang M-Z, Cournède P-H, Mathieu A, Letort V, Qi R, Zhan Z-G.** 2009. A functional-structural plant model—Theories and its applications in agronomy. In: Cao W, White JW, Wang E, eds. *Crop modeling and decision support*. Berlin, Heidelberg: Springer, 148–160.
- Kellogg EA.** 2007. Floral displays: genetic control of grass inflorescences. *Current Opinion in Plant Biology* **10**, 26–31.
- Kirchoff BK, Claßen-Bockhoff R.** 2013. Inflorescences: concepts, function, development and evolution. *Annals of Botany* **112**, 1471–1476.
- Klein LL, Miller AJ, Ciotir C, Hyma K, Uribe-Convers S, Londo J.** 2018. High-throughput sequencing data clarify evolutionary relationships among North American *Vitis* species and improve identification in USDA *Vitis* germplasm collections. *American Journal of Botany* **105**, 215–226.
- Kuijt J.** 1981. Inflorescence morphology of Loranthaceae. *Blumea* **27**, 1–73.
- Kumar S, Stecher G, Li M, Knyaz C, Tamura K.** 2018. MEGA X: molecular evolutionary genetics analysis across computing platforms. *Molecular Biology and Evolution* **35**, 1547–1549.
- Landrein S, Prender G, Chase MW, Clarkson JJ.** 2012. *Abelia* and relatives: phylogenetics of Linnaeae (Dipsacales–Caprifoliaceae s.l.) and a new interpretation of their inflorescence morphology. *Botanical Journal of the Linnean Society* **169**, 692–713.
- Le C-T, Liu B, Barrett RL, Lu L-M, Wen J, Chen Z-D.** 2018. Phylogeny and a new tribal classification of Opiliaceae (Santalales) based on molecular and morphological evidence: phylogeny and classification of Opiliaceae. *Journal of Systematics and Evolution* **56**, 56–66.
- Letort V, Cournede P, Lecoeur J, Hummel I, Reffye PD, Christophe A.** 2006. Effect of topological and phenological changes on biomass partitioning in *Arabidopsis thaliana* inflorescence: a preliminary model-based study. In: Thierry F, Zhang XP, eds. *Plant growth modeling, simulation, visualization and application*. IEEE Computer Society, 65–69.
- Li M, An H, Angelovici R, et al.** 2018a. Topological data analysis as a morphometric method: using persistent homology to demarcate a leaf morphospace. *Frontiers in Plant Science* **9**, 553.
- Li M, Duncan K, Topp CN, Chitwood DH.** 2017. Persistent homology and the branching topologies of plants. *American Journal of Botany* **104**, 349–353.
- Li M, Frank MH, Coneva V, Mio W, Chitwood DH, Topp CN.** 2018b. The persistent homology mathematical framework provides enhanced genotype-to-phenotype associations for plant morphology. *Plant Physiology* **177**, 1382–1395.
- Marguerit E, Boury C, Manicki A, Donnart M, Butterlin G, Némorin A, Wiedemann-Merdinoglu S, Merdinoglu D, Ollat N, Decroocq S.** 2009. Genetic dissection of sex determinism, inflorescence morphology and downy mildew resistance in grapevine. *Theoretical and Applied Genetics* **118**, 1261–1278.
- Mathers AW, Hepworth C, Baillie AL, Sloan J, Jones H, Lundgren M, Fleming AJ, Mooney SJ, Sturrock CJ.** 2018. Investigating the micro-structure of plant leaves in 3D with lab-based X-ray computed tomography. *Plant Methods* **14**, 99.
- McAllister CA, McKain MR, Li M, Bookout B, Kellogg EA.** 2019. Specimen-based analysis of morphology and the environment in ecologically dominant grasses: the power of the herbarium. *Philosophical Transactions of the Royal Society B: Biological Sciences* **374**, 20170403.
- Migicovsky Z, Li M, Chitwood DH, Myles S.** 2017. Morphometrics reveals complex and heritable apple leaf shapes. *Frontiers in Plant Science* **8**, 2185.
- Miller AJ, Matasci N, Schwaninger H, Aradhya MK, Prins B, Zhong GY, Simon C, Buckler ES, Myles S.** 2013. *Vitis* phylogenomics: hybridization intensities from a SNP array outperform genotype calls. *PLoS One* **8**, e78680.
- Molitor D, Behr M, Hoffmann L, Evers D.** 2012. Impact of grape cluster division on cluster morphology and bunch rot epidemic. *American Journal of Enology and Viticulture* **63**, 508–514.
- Molitor D, Beyer M.** 2014. Epidemiology, identification and disease management of grape black rot and potentially useful metabolites of black rot pathogens for industrial applications – a review. *The Annals of Applied Biology* **165**, 305–317.
- Molitor D, Biewers B, Junglen M, et al.** 2018. Multi-annual comparisons demonstrate differences in the bunch rot susceptibility of nine *Vitis vinifera* L. ‘Riesling’ clones. *Vitis* **57**, 17–25.
- Moore MO.** 1991. Classification and systematics of eastern North American *Vitis* L. (Vitaceae) north of Mexico. *SIDA, Contributions to Botany* **14**, 339–367.
- Moore M, Wen J.** 2016. Vitaceae. In: Flora of North America Editorial Committee, ed. *Flora of North America North of Mexico*, Vol. 12, Magnoliophyta: Vitaceae to Garryaceae. Oxford, New York: Oxford University Press, 3–23.
- Morris GP, Ramu P, Deshpande SP, et al.** 2013. Population genomic and genome-wide association studies of agroclimatic traits in sorghum. *Proceedings of the National Academy of Sciences, USA* **110**, 453–458.
- Mullins MG, Bouquet A, Williams LE.** 1992. *Biology of the grapevine*. Cambridge: Cambridge University Press.
- Munson TV.** 1909. *Foundations of American Grape culture*. New York: Orange Judd Company.
- OIV.** 2001. OIV Descriptor list for grape varieties and *Vitis* species, 2nd edn. Paris: Organisation Internationale de la Vigne et du Vin.
- Périalleux C, Lobet G, Tocquin P.** 2014. Inflorescence development in tomato: gene functions within a zigzag model. *Frontiers in Plant Science* **5**, 121.
- Pfeifer J, Kirchgessner N, Colombi T, Walter A.** 2015. Rapid phenotyping of crop root systems in undisturbed field soils using X-ray computed tomography. *Plant Methods* **11**, 41.
- Poni S, Gatti M, Palliotti A, et al.** 2018. Grapevine quality: a multiple choice issue. *Scientia Horticulturae* **234**, 445–462.
- Prusinkiewicz P, Erasmus Y, Lane B, Harder LD, Coen E.** 2007. Evolution and development of inflorescence architectures. *Science* **316**, 1452–1456.
- Pulliat V.** 1888. *Mille variétés de vignes, description et synonymies*. Paris Montpellier: Coulet, Delahaye et Crosnier.
- Reeve AL, Skinkis PA, Vance AJ, McLaughlin KR, Tomasino E, Lee J, Tarara JM.** 2018. Vineyard floor management and cluster thinning inconsistently affect ‘Pinot noir’ crop load, berry composition, and wine quality. *HortScience* **53**, 318–328.
- Revell LJ.** 2012. phytools: an R package for phylogenetic comparative biology (and other things). *Methods in Ecology and Evolution* **3**, 217–223.
- Richter R, Gabriel D, Rist F, Töpfer R, Zyprian E.** 2019. Identification of co-located QTLs and genomic regions affecting grapevine cluster architecture. *Theoretical and Applied Genetics* **132**, 1159–1177.
- Rist F, Herzog K, Mack J, Richter R, Steinlage V, Töpfer R.** 2018. High-precision phenotyping of grape bunch architecture using fast 3D sensor and automation. *Sensors* **18**, 763.
- Rombough L.** 2002. *The grape grower: a guide to organic viticulture*. White River Junction, VT, USA: Chelsea Green Publishing.
- Roscher R, Herzog K, Kunkel A, Kicherer A, Töpfer R, Förstner W.** 2014. Automated image analysis framework for high-throughput determination of grapevine berry sizes using conditional random fields. *Computers and Electronics in Agriculture* **100**, 148–158.
- Rovasenda J.** 1881. *Essai d'une ampélographie universelle*. Traduit de l'italien par F. Cazalis, G. Foëx et al.
- Shavrukov YN, Dry IB, Thomas MR.** 2004. Inflorescence and bunch architecture development in *Vitis vinifera* L. *Australian Journal of Grape and Wine Research* **10**, 116–124.
- Stitzer MC, Ross-Ibarra J.** 2018. Maize domestication and gene interaction. *New Phytologist* **220**, 395–408.
- Swofford DL.** 2003. PAUP\*: phylogenetic analysis using parsimony, version 4.0b10. Sunderland, MA, USA: Sinauer Associates.

- Symonova O, Topp CN, Edelsbrunner H.** 2015. DynamicRoots: a software platform for the reconstruction and analysis of growing plant roots. *PLoS One* **10**, e0127657.
- Ta KN, Khong NG, Ha TL, et al.** 2018. A genome-wide association study using a Vietnamese landrace panel of rice (*Oryza sativa*) reveals new QTLs controlling panicle morphological traits. *BMC Plant Biology* **18**, 282.
- Tello J, Aguirrezaábal R, Hernáiz S, Larreina B, Montemayor MI, Vaquero E, Ibáñez J.** 2015. Multicltivar and multivariate study of the natural variation for grapevine bunch compactness: multicltivar study of grapevine bunch compactness. *Australian Journal of Grape and Wine Research* **21**, 277–289.
- Tello J, Ibáñez J.** 2018. What do we know about grapevine bunch compactness? A state-of-the-art review: Review on bunch compactness. *Australian Journal of Grape and Wine Research* **24**, 6–23.
- Tröndle D, Schröder S, Kassmeyer HH, Kiefer C, Koch MA, Nick P.** 2010. Molecular phylogeny of the genus *Vitis* (Vitaceae) based on plastid markers. *American Journal of Botany* **97**, 1168–1178.
- Venables WN, Ripley BD.** 2002. Modern applied statistics with S, 4th edn. New York: Springer.
- Weberling F.** 1992. Morphology of flowers and inflorescences. Cambridge: Cambridge University Press.
- Wei T, Simko V.** 2017. R package ‘corrplot’: visualization of a correlation matrix (version 0.84). <https://github.com/taiyun/corrplot>.
- Whipple CJ.** 2017. Grass inflorescence architecture and evolution: the origin of novel signaling centers. *New Phytologist* **216**, 367–372.
- Wyatt R.** 1982. Inflorescence architecture: how flower number, arrangement, and phenology affect pollination and fruit-set. *American Journal of Botany* **69**, 585–594.
- Zdunić G, Mucalo A, Budić-Leto I, Humar I, Pejić I, Maletić E.** 2015. Cluster architecture of old, neglected Croatian grapevine varieties (*Vitis vinifera* L.). *Vitis* **54**, 177–180.
- Zecca G, Abbott JR, Sun WB, Spada A, Sala F, Grassi F.** 2012. The timing and the mode of evolution of wild grapes (*Vitis*). *Molecular Phylogenetics and Evolution* **62**, 736–747.
- Zhang N, Wen J, Zimmer EA.** 2015. Expression patterns of AP1, FUL, FT and LEAFY orthologs in Vitaceae support the homology of tendrils and inflorescences throughout the grape family: evolution of tendrils in Vitaceae. *Journal of Systematics and Evolution* **53**, 469–476.